Inefficient clearance of myelin debris by microglia impairs remyelinating processes

Antoine Lampron,[1]* Antoine Larochelle,[1]* Nathalie Laflamme,[1] Paul Préfontaine,[1] Marie-Michèle Plante,[1] Maria Gabriela Sánchez,[1] V. Wee Yong,[2] Peter K. Stys,[2] Marie-Ève Tremblay,[1] and Serge Rivest[1]

[1]Department of Molecular Medicine, Faculty of Medicine, Neuroscience Laboratory, CHU de Québec Research Center, Laval University, Quebec City, Quebec 2G1V 4G2, Canada
[2]Department of Clinical Neurosciences and the Hotchkiss Brain Institute, University of Calgary, Calgary, Alberta T2N 4N1, Canada

An imbalance between remyelinating and demyelinating rates underlies degenerative processes in demyelinating diseases such as multiple sclerosis. An optimal therapeutic strategy would be to stimulate remyelination while limiting demyelination. Although accumulation of myelin debris impairs remyelination, the mechanisms regulating the clearance of such debris by mononuclear phagocytic cells are poorly understood. We demonstrate that after cuprizone intoxication, CCR2-dependent infiltration of mouse bone marrow–derived cells is abundant in demyelinating areas, but that these cells do not impact demyelination. However, in CX3CR1-deficient mice, the clearance of myelin debris by microglia was blocked greatly, affecting the integrity of the axon and myelin sheaths and thus preventing proper remyelination. These results highlight the crucial role played by CX3CR1 in myelin removal and show that there can be no efficient remyelination after a primary demyelinating insult if myelin clearance by microglia is impaired.

CORRESPONDENCE
Serge Rivest:
serge.rivest@crchudequebec.ulaval.ca

Abbreviations used: BBB, blood–brain barrier; BMDC, BM-derived cells; EAE, experimental autoimmune encephalomyelitis; FJB, Fluoro-Jade B; IBA1, anti-ionized calcium binding adaptor molecule 1; MDM, monocyte-derived macrophages; OD, oligodendrocytes; OPC, oligodendrocyte precursor cells; PDGFRα, platelet-derived growth factor receptor α; PFA, paraformaldehyde.

Multiple sclerosis (MS) is a chronic inflammatory disorder of the central nervous system (CNS) associated with prominent demyelination, which impairs the conduction of signals along axons (Lublin et al., 2014). Whereas the therapeutic control of immune processes has proven efficient to limit the relapsing–remitting form of MS, the current immunomodulatory treatments have failed to prevent patients from entering a progressive course of the disease or to limit disease progression in this phase (Lublin and Reingold, 1996; Lassmann et al., 2012). Remyelination is the natural regenerative mechanism to counter demyelination (Franklin and Ffrench-Constant, 2008), but the reasons why remyelination fails or is incomplete during MS are not completely understood (Goldschmidt et al., 2009). There is a need for better knowledge of the mechanisms underlying remyelination to develop long-term regenerative therapeutic options for patients affected by demyelinating disorders.

Myelin removal is a critical step in the remyelination process (Kotter et al., 2006). Cells of the mononuclear phagocytic system, including monocyte-derived macrophages (MDM) and microglia, are actively implicated in the clearance of myelin debris (Napoli and Neumann, 2010). Microglia are resident macrophages of the CNS that originate from progenitors in the embryonic yolk sac populating the brain during early embryogenesis (Ginhoux et al., 2010; Schulz et al., 2012). Monocytes are macrophage precursors in the circulation and derive from BM progenitors (Geissmann et al., 2010). Although monocytes do not migrate into the CNS under normal conditions, we and others have shown the specific infiltration of MDMs under pathological conditions (Shechter et al., 2009; Ajami et al., 2011; Lampron et al., 2013; Bellavance et al., 2014). Microglia and macrophages are regarded as detrimental in MS and experimental autoimmune encephalomyelitis (EAE) because of their roles in autoimmunity, such as antigen presentation and proinflammatory cytokine production (Fife et al., 2000;

*A. Lampron and A. Larochelle contributed equally to this paper.

The Rockefeller University Press $30.00
J. Exp. Med. 2015 Vol. 212 No. 4 481–495
www.jem.org/cgi/doi/10.1084/jem.20141656

The Journal of Experimental Medicine

Heppner et al., 2005; Ajami et al., 2011). However, these noxious roles might mask other beneficial properties. During demyelination, microglia exert a phenotype associated with phagocytosis and the recruitment of oligodendrocyte precursor cells (OPCs; Jurevics et al., 2002; Olah et al., 2012). Whereas recent work unraveled differences between the roles played by blood-borne macrophages and microglia during autoimmune-mediated demyelination (Yamasaki et al., 2014), their respective functions in the process of primary de- and remyelination of the brain are not completely understood. Furthermore, it remains to be determined whether circulating monocytes can engraft the brain and differentiate into macrophages during demyelination in the absence of blood–brain barrier (BBB) damages (McMahon et al., 2002; Mildner et al., 2007; Remington et al., 2007).

Cuprizone is a copper chelating toxin that induces apoptosis of oligodendrocytes (OD) when added to standard rodent chow. Cuprizone induces apoptosis of ODs during the first 3 wk, which leads to massive demyelination accompanied by significant recruitment of OPC, astrogliosis, and microgliosis (Hiremath et al., 1998; Gudi et al., 2014). After removal of cuprizone from the diet, complete remyelination of affected sites occurs over the course of 1–3 wk. It has become a prime model to study both autoimmune-independent demyelination in the absence of BBB disruption (Arnett et al., 2001; Matsushima and Morell, 2001) and the action of remyelinating agents such as OD cell stimulants (Deshmukh et al., 2013). Here, we used the cuprizone model to study the differential roles played by monocytes versus microglia during demyelination and remyelination. Although significant recruitment of monocytes from the circulation to the demyelinating sites occurs during the demyelination phase, these cells do not impact de- or remyelination. However, we show that CX3CR1-dependent mechanisms are crucial for the efficient clearance of degenerating myelin by microglia after OD death. This clearance is necessary for the successful remyelination of axons. These results pave the way for a host of new therapeutic options for demyelinating diseases through boosting the clearance of degenerate myelin, which allows for more efficient remyelination of the affected sites.

RESULTS

Cuprizone induces a CCR2-dependent recruitment of peripheral cells into the CNS

In the cuprizone model, CNS infiltration of BM-derived cells (BMDCs) has been reported by generating chimeric mice using total body irradiation coupled with BM transplantation (McMahon et al., 2002). However, the current understanding of the subject is that irradiation along with BM transplantation induces unwanted infiltration of cells into the CNS of untreated healthy animals and compelling evidence has demonstrated that this infiltration is not a physiological process (Ajami et al., 2007; Mildner et al., 2007). To address this issue, BM cells extracted from either $GFP^{+/-}$ or $CCR2^{-/-}$ donor mice were injected into the tail vein of mice pretreated with a busulfan/cyclophosphamide (BuCy) based chemotherapy regimen (Fig. 1 A). This regimen leads to a strong chimerism (>90%) in the circulation (Fig. 1 B) but does not induce artificial infiltration of BMDCs into the CNS under physiological conditions (Fig. 1 D) as expected (Lampron et al., 2012). 6 wk after transplantation, cuprizone supplemented chow was given to these mice that were sacrificed at various time points (Fig. 1 A). A significant infiltration of peripheral cells into the CNS was observed, with a peak of infiltration at weeks 4 and 5 of treatment (Fig. 1 C). Infiltrated cells were attracted to the sites of demyelinated white matter, most notably the corpus callosum (CC; Fig. 1 E) and striatum, but not the cerebellum (unpublished data). This infiltration was transient, as limited numbers of GFP^+ cells were seen after 6 wk of treatment and even less when regular chow was reintroduced for 2 wk (Fig. 1 C, RM). The knockout of CCR2 in the periphery abrogated the infiltration of BMDCs into the CNS of cuprizone-fed mice by 96% (Fig. 2, A and C). 81% of infiltrated cells were also positive for microglial marker Iba1 (Fig. 2, A and B) and also expressed CD68, a marker of the myeloid lineage (Pulford et al., 1990; not depicted). A lower proportion of the few (<30) GFP^+ cells detected in $CCR2^{-/-}$ chimeric mice were Iba1 positive (38%, Figs. 1 F and 2 A). T cell marker CD3 was detected in few GFP+ cells found in $CCR2^{-/-}$ and GFP chimeric mice (data not shown). F4/80-immunoreactivity (ir) signal was also detected in a low proportion of infiltrating cells (Fig. 2, D and E). Black Gold staining was used to measure the area of demyelination in the CC of these animals after 6 wk of cuprizone diet (Fig. 3, A and B) or the extent of remyelination when regular chow was reintroduced for 2 wk (Fig. 3 C). There was extensive demyelination of the CC in both GFP and $CCR2^{-/-}$ chimeric mice (Fig. 3 A). Peripheral $CCR2^{-/-}$ knockout and the blockade of BMDC infiltration into the CNS did not impact the subsequent remyelination either (Fig. 3 C). These results show that there is a regulated recruitment of monocytes to the sites of demyelination in the cuprizone model, but that these CCR2-expressing cells seem to have little impact on the demyelination or remyelination processes.

Significant impact of CX3CR1 knockout on cuprizone-induced demyelination

Although infiltration of CCR2-expressing cells did not have a significant impact on the demyelination induced by cuprizone feeding (Fig. 1–3), there is a robust accumulation of microglial cells at the sites of demyelination throughout the cuprizone protocol (Fig. 1, E–F) and their importance has been hinted at for many years (Gudi et al., 2014). CX3CR1 is a crucial receptor controlling microglial physiology and orchestrating the crosstalk between microglia and neurons that constitutively express its sole known ligand, fractalkine (CX3CL1) (Imai et al., 1997; Bellavance et al., 2014; Paolicelli et al., 2014). Remarkably, CX3CR1-deficient mice seemed almost immune to cuprizone as histochemical staining of myelin in these mice revealed a very mild level of demyelination in the CC when compared with WT littermates at 3 and 5 wk (Fig. 4, A and B). However, both genotypes exhibited similar

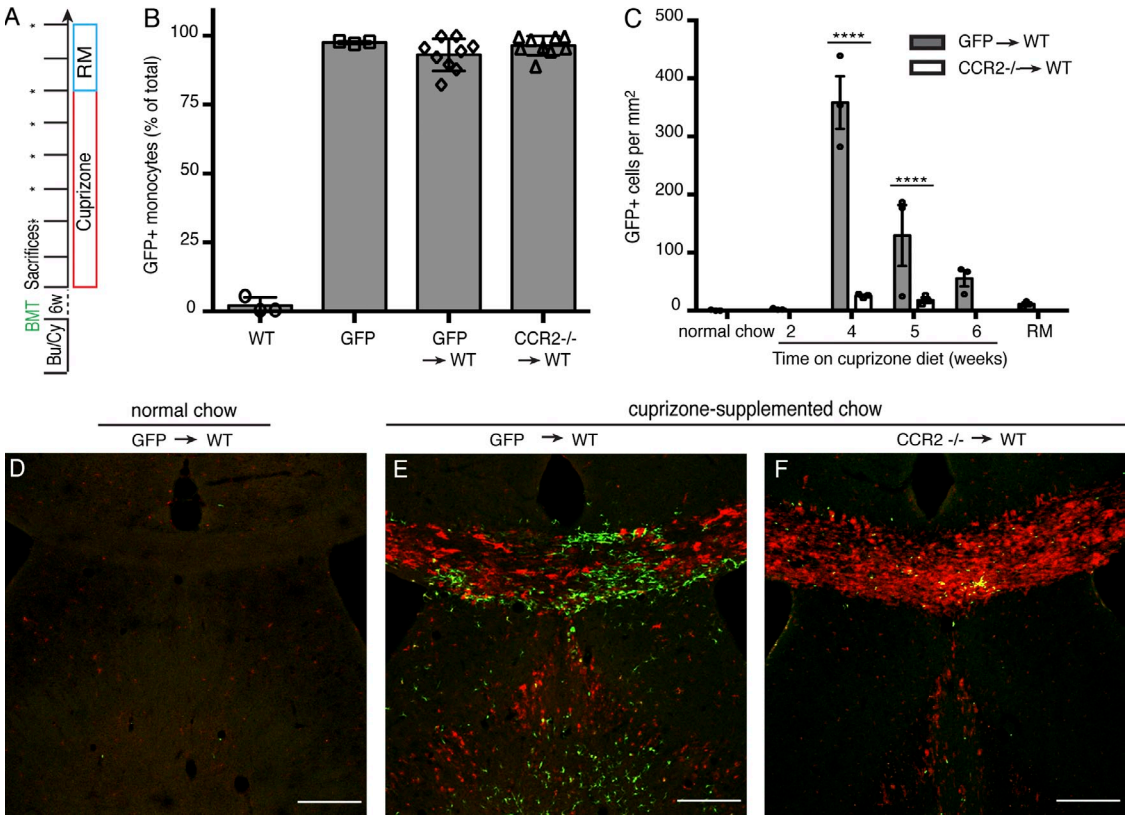

Figure 1. BM-derived cells are recruited in a CCR2-dependent manner into demyelinating sites of the CNS in the cuprizone model. (A) A Busulfan/Cyclophosphamide chemotherapy regimen was used to prepare WT mice to receive the injection of BM cells from GFP$^{+/-}$ mice. 6 wk after transplantation, 0.2% Cuprizone was added to the diet for up to 6 wk. Mice were sacrificed after 2, 3, 4, 5, and 6 wk on a cuprizone-supplemented diet. Another group was sacrificed 2 wk after removing cuprizone from the diet to allow remyelination. (B) Flow cytometry analysis of GFP expression in circulating monocytes of WT mice, GFP$^{+/-}$ mice, chimeric GFP → WT mice, and and CCR2$^{-/-}$ → WT mice. (C) GFP^{+} cells were counted with a stereologic apparatus. Reported is the total number of GFP^{+} cells per slice counted per animal. (D-F) Representative confocal images of GFP^{+} cells (green) and immunoreactive Iba1^{+} cells (red) in the hippocampus and corpus callosum of chimeric mice either untreated (D) or after 5 wk of treatment with a cuprizone diet in GFP (E) and CCR2$^{-/-}$ (F) chimeric mice. One representative experiment out of two is shown. *n* = 3–9 mice/group. ****, P < 0.0001. Bars, 100 µm.

behavioral defects as measured by the time spent in the open arm of an elevated plus maze (Fig. 4 C). Food intake and weight changes (Fig. S1, A and B) were monitored throughout the protocols and no difference could be found between WT and CX3CR1$^{-/-}$ mice, showing that the difference between genotypes was not attributable to differential metabolic responses to a cuprizone-supplemented diet. Cuprizone treatment leads to a specific depletion of ODs in the CNS (Bénardais et al., 2013). Stereologic assessment of the number of mature ODs in the CC showed a similar depletion of ODs (Fig. 4 D). Furthermore, electron microscopy imaging similarly showed apoptotic ODs in CX3CR1$^{-/-}$ mice (Fig. 4 E). Thus, preservation of myelin in CX3CR1 knockout mice does not result from increased survival of ODs in these mice, as these cells die by apoptosis at a similar extent to what's observed in WT mice exposed to cuprizone.

Microglial activity in CX3CR1$^{-/-}$ mice

In the CNS, CX3CR1 is expressed exclusively by microglia and perivascular macrophages (Cardona et al., 2006). Because infiltrating CCR2 cells had limited effects on cuprizone-induced demyelination (Fig. 1–3) and CX3CR1 knockout did not impact metabolic processes or OD death (Fig. 4, D and E), we hypothesized a deficient microglial activity to be responsible for the protective effect on myelin content observed against cuprizone in CX3CR1-deficient mice. Although the CC of CX3CR1$^{-/-}$ mice showed lower Iba1 immunoreactivity than WT mice (Fig. 5 A), a massive infiltration of the region by microglia is still observed when compared with littermates fed with a normal chow (Fig. 5 A). To characterize the inflammatory response in each genotype, we determined the expression level in the CC of TLR2 and C1q-α, markers of NF-κB–induced or complement-activated inflammatory processes, respectively. As expected, a robust and significant induction of both genes was noted in WT mice comparable to that observed in CX3CR1$^{-/-}$ mice (Fig. 5, B and C), showing no significant difference in the inflammatory reaction between genotypes. However, the expression of the gene encoding for TREM2, a protein involved in phagocytosis (Takahashi et al., 2005), was much lower in CX3CR1$^{-/-}$

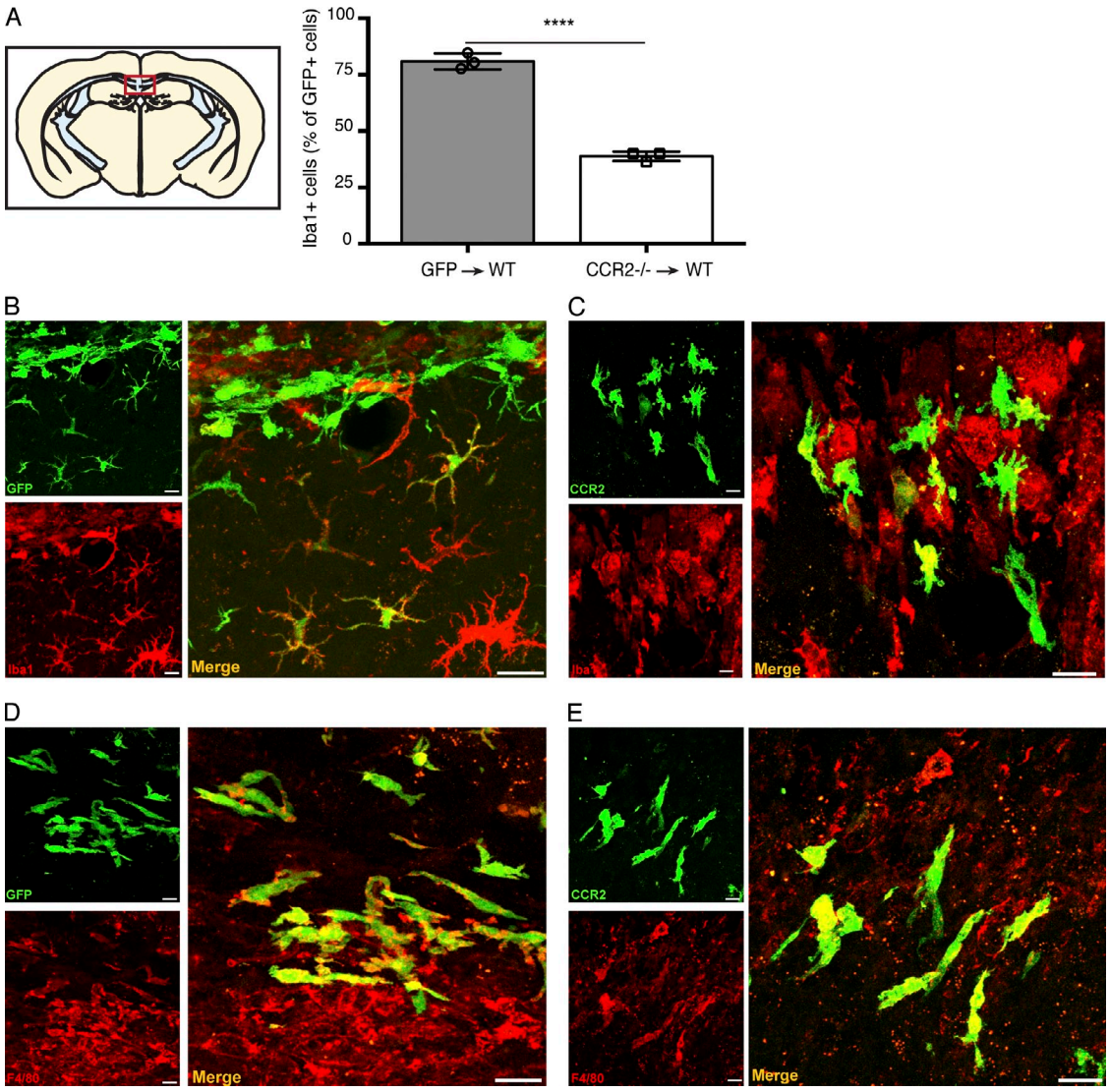

Figure 2. Infiltrated cells are immunoreactive for macrophage markers. (A) The diagram represents a coronal section where the pictures in B–E were taken (red box). Iba1 immunostaining was performed on brain sections from GFP → WT and CCR2$^{-/-}$ → WT chimeric mice. Proportion of GFP^{+} cells that were also Iba1^{+} after 4 wk of treatment as counted on the stereological apparatus. (B–E) Representative confocal images reveal apparent co-localization of GFP (green) with Iba1 (red; B and C) and F4/80 (red; D and E) in the corpus callosum of GFP → WT (B and D) and CCR2$^{-/-}$ → WT chimeric mice (C and E). Merged images are also shown. One representative experiment out of two is shown. n = 4–5 mice/group. ****, $P < 0.0001$ from an unpaired two-tailed Student's t test. Bars, 20 µm.

than in WT mice (Fig. 6 A). As a protein implicated in antigen presentation, the induction of CD11c in microglia is also indicative of the phagocytic activity of microglia. Flow cytometry analysis of the expression of CD11c on live CD45^{+}CD11b^{+} cells in the CNS (Fig. 6 B) revealed a similar pattern of expression, as its induction was lower in CX3CR1$^{-/-}$ mice than in WT littermates (Fig. 6 C). Electron microscopy imaging of Iba1-stained microglia (Fig. 6, D and E) confirmed these observations as WT microglia showed extensive accumulation of nonstained endosomes (Fig. 6 D, red arrow), myelin products often partially digested and localized within the endosomes (Fig. 6 D, green arrow), and cholesterol crystals inside of their cytoplasm (Fig. 6 D, blue arrow). However, microglia in CX3CR1$^{-/-}$ mice were almost devoid of endosomes, internalized myelin, and cholesterol crystals (Fig. 6 E), suggesting a reduced phagocytic activity in the CX3CR1$^{-/-}$ mice (Tangirala et al., 1994; Klinkner et al., 1995; Lindberg et al., 2014). Collectively, these results show that although inflammatory responses are not affected by the knockout of CX3CR1, there is a clear deficit in microglial phagocytic processes.

Aberrant myelin patterns in CX3CR1$^{-/-}$ mice

A robust recruitment of microglia takes place in demyelinating regions of WT mice, but this phenomenon was attenuated in CX3CR1$^{-/-}$ mice after both 3 (Fig. 7, A and B) and 5 (Fig. 7, C and D) weeks of cuprizone. It is interesting to

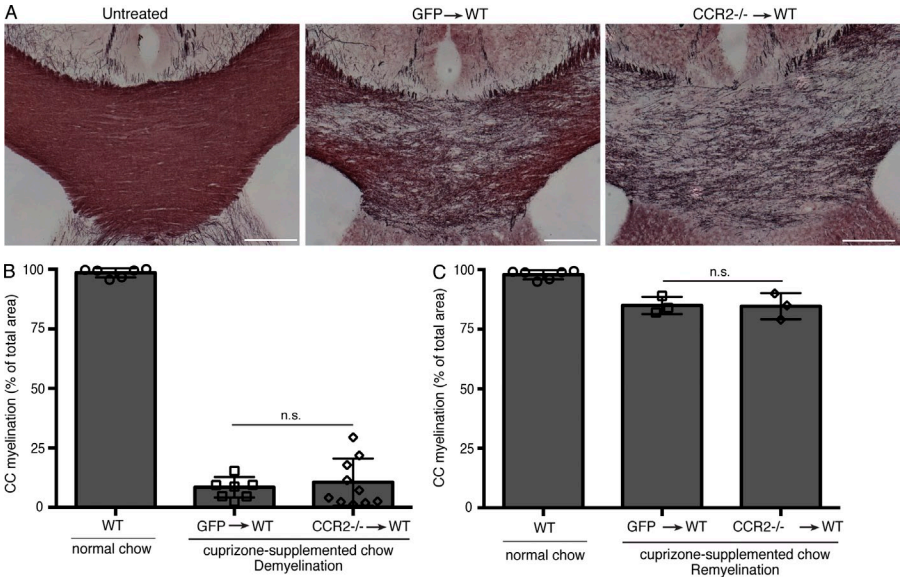

Figure 3. Infiltration of BMDCs into the CNS in the cuprizone model does not impact demyelination or remyelination. (A) Staining of myelin with Black Gold II was performed on brain sections from GFP → WT and CCR2$^{-/-}$ → WT chimeric mice. Representative micrograph images show Black Gold staining of untreated (left), GFP → WT (middle), and CCR2 → WT (right) chimeric mice after 6 wk of treatment with cuprizone or normal chow. (B and C) Demyelination (B) and remyelination (C) were measured in the corpus callosum of either GFP → WT or CCR2$^{-/-}$ → WT after 6 wk of treatment with cuprizone (B) or 2 wk of normal chow after 6 wk of cuprizone (C). Differences between the GFP and CCR2$^{-/-}$ groups were found not significant, with adjusted p-values over 0.8 in both cases in a one-way ANOVA followed by Turkey post-hoc test for multiple comparisons. One representative experiment out of two is shown. n = 3–10 mice/group. Bars, 100 µm.

note the presence of myelin debris in these microglia, especially in WT animals, suggesting a potent phagocytic response by these cells. Such a response by microglia is clearly weakened in CX3CR1$^{-/-}$ (Video 1). In the CX3CR1$^{-/-}$ mice, additional analysis of myelin patterns by electron microscopy revealed abundant myelin aberrations throughout sections of the CC (Fig. 7, G and J–M). Large, round, and empty myelin-enclosed structures reminiscent of spheroids, a hallmark of MS (Ferguson et al., 1997; Trapp et al., 1998) and found in other models of CNS pathology (Stirling et al., 2013), were also observed (Fig. 7 M). Whereas some aberrations were present in WT mice, spheroid-like structures were not observed in these mice. As such, it appears that disrupting myelin clearance by microglia leads to myelin disorganization and that deleting CX3CR1 is not a protective mechanism, as first suggested by the histochemical staining (Fig. 4 A). These results prompted the analysis of remyelinating processes in the case of inefficient clearance of aberrant myelin patterns, sacrificing mice 1 and 2 wk after cuprizone was removed from 6 wk diet. OPCs are normally recruited to the demyelinated CC from the beginning of week 4 to the end of week 5 (Blakemore and Irvine, 2008). As a marker of the earliest OD progenitors, PDGFRα expression was assessed by in situ hybridization, which revealed a significantly lowered level of induction of this gene in CX3CR1$^{-/-}$ mice after 4 wk of cuprizone (Fig. 8, A and B) and by immunohistochemistry after 5 wk of cuprizone (Fig. 8 E). Furthermore, stereologic assessment of Olig2^{+} cells confirmed a deficient recruitment of OPCs in CX3CR1$^{-/-}$ mice at 5 wk (Fig. 8, C and D). Proliferating OPCs were determined by the presence of Ki67 staining in Olig2^{+} cells in the brain of WT mice, a phenomenon that was marginal in the CC of CX3CR1$^{-/-}$ mice (Fig. 8 E). This was also associated with a low PDGFRα-ir and IGF-1-ir signal, suggesting a defect in the mechanisms that trigger OPC proliferation in the CC of CX3CR1$^{-/-}$ (Fig. 8 E). Surprisingly, Black Gold staining showed efficient remyelination of the CC in both WT and CX3CR1$^{-/-}$ mice, although myelin-positive staining remained lower in WT mice at 1 wk after the cuprizone diet was replaced by normal chow (Fig. 9 A). Electron microscopy analysis of myelin integrity revealed another set of aberrant patterns, including myelin disorganization, separation of myelin layers, hypermyelination, vacuolization of axons, and a persistence of large spheroid-like structures (Fig. 9 B). Although 14.6% of axons displayed some of these patterns (but not spheroids) in WT mice, the frequency of aberrantly myelinated axons reached 67.9% in CX3CR1$^{-/-}$ mice ($P < 0.0001$; Fig. 9 C). Collectively, these results show that impaired clearance of myelin by microglia through CX3CR1 depletion leads to deficits in myelin organization creating defective remyelination of axons in the cuprizone model.

DISCUSSION

Skewing the balance toward remyelination is a key goal for the long-term treatment of patients with demyelinating diseases such as MS. In this study, we used the toxin cuprizone to model a primary demyelinating insult and to study the impact of monocytes and microglia on demyelination and remyelination. We have shown that monocytes from the periphery can enter the CNS at demyelinating sites, but that these infiltrating cells do not significantly impact the processes of demyelination or remyelination. However, knocking out CX3CR1 severely impeded phagocytosis of myelin by microglia, leading to the persistence of myelin debris throughout the white matter of cuprizone-fed mice. This resulted in inefficient axonal remyelination characterized with

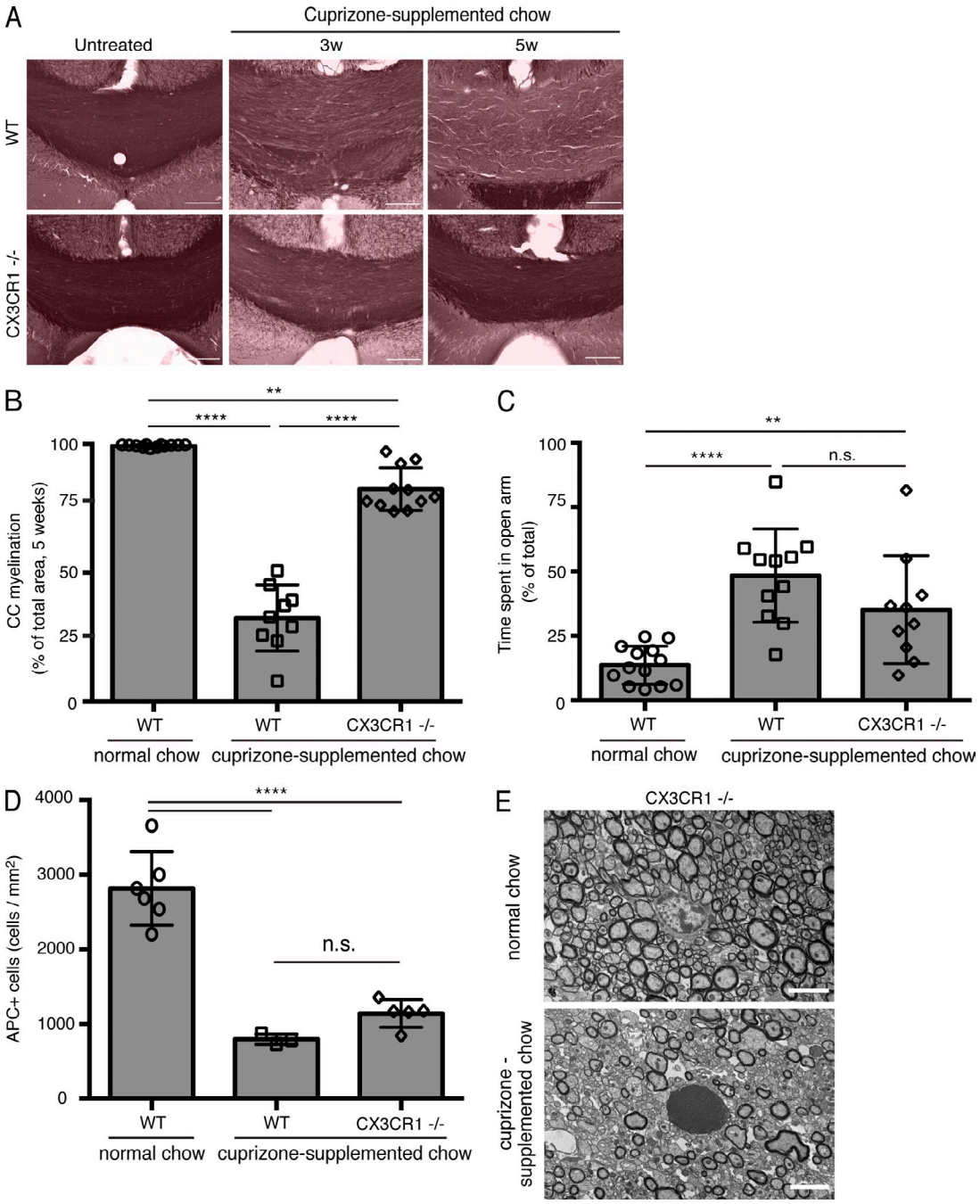

Figure 4. CX3CR1 knockout severely impacts cuprizone-induced demyelination. (A) Staining of myelin with Black Gold II was performed on brain sections from WT and CX3CR1$^{-/-}$ mice 3 and 5 wk after the cuprizone treatment or normal chow. Representative photomicrographs are shown. (B) Quantification of demyelination was measured in the corpus callosum using a stereological procedure 5 wk after normal chow or cuprizone treatment in WT and CX3CR1$^{-/-}$ mice. (C) Time spent in the open arm of the elevated plus maze behavioral test, efficient to assess behavioral deficits induced by cuprizone (Lister, 1987). (D) Stereologic assessment of APC^{+} cells in the corpus callosum of WT and CX3CR1$^{-/-}$ mice after 5 wk of a cuprizone-supplemented diet or normal chow. APC is a specific marker for mature myelinating oligodendrocytes. (E) Representative electron microscopy images of oligodendrocytes in the corpus callosum of CX3CR1$^{-/-}$ mice, either untreated, or after 6 wk of a cuprizone-supplemented diet. One representative experiment out of two is shown. n = 4–12 mice/group. (B) **, P = 0.002; ****, P < 0.0001; (C and D) **, P = 0.0093; ****, P < 0.0001. Bars: (A) 100 µm; (E) 2 µm.

aberrant myelin patterns, thus demonstrating the critical role of CX3CR1 in promoting microglial clearance of degenerate myelin and its importance for an efficient remyelination of demyelinating sites.

Infiltration of circulating myeloid cells to sites of demyelination has been reported in earlier studies (McMahon et al., 2002; Remington et al., 2007). These studies used irradiation-conditioned chimeric mice or flow cytometry to dissociate

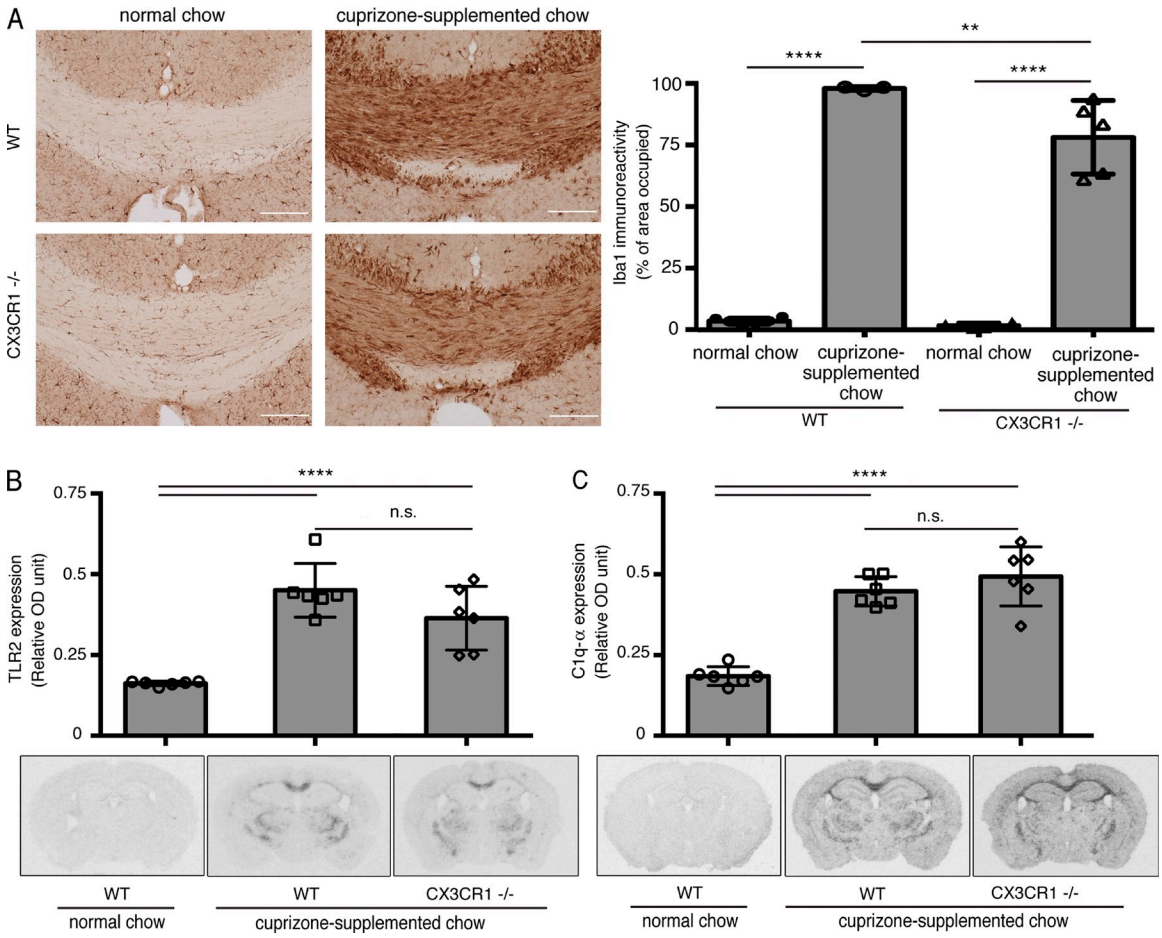

Figure 5. Cuprizone treatment triggered microgliosis and inflammation in the corpus callosum of mice in a CX3CR1-independent manner. (A) Iba1 was immunostained on brain sections from WT and CX3CR1$^{-/-}$ mice after 4 wk of normal show or a cuprizone-supplemented diet, the peak time point for microglial accumulation in the corpus callosum. Representative Iba1 immunostaining photomicrographs in the corpus callosum. The area covered by Iba1^{+} staining was measured in the corpus callosum using a stereological procedure (right). (B and C) TLR2 and C1qα mRNA was hybridized on brain sections from WT and CX3CR1$^{-/-}$ mice after 4 wk of treatment with cuprizone or normal show. Semiquantitative expression levels of TLR2 (B) and C1q-α (C) mRNA signal were measured in the corpus callosum using ImageJ. The coronal sections at the bottom depict representative images of TLR2 (B) and C1q-α (C) in situ hybridization signal. One representative experiment out of two is shown. n = 3–6 mice/group. **, P = 0.01; ****, P < 0.001. Bars: (A) 100 µm.

between macrophages and microglia. A study using head-protected, irradiation-conditioned, GFP chimeric mice questioned these results (Mildner et al., 2007). The authors of that study showed that peripheral macrophage infiltration does not occur when the head is protected during irradiation and concluded that cell recruitment to the CC during cuprizone-induced demyelination is an artifact resulting from irradiation-related side effects, namely BBB dysfunction and neuroinflammation. The cuprizone model induces a severe demyelination of specific sites, whereas the BBB remains intact as demonstrated by several studies (Bakker and Ludwin, 1987; Kondo et al., 1987; Matsushima and Morell, 2001). In our study, we showed that recruitment occurs when chimeric mice are generated using a chemotherapeutic conditioning, a procedure we have demonstrated to maintain BBB integrity and to be nonpermissive for the entry of cells into the CNS (Lampron et al., 2012; Michaud et al., 2013; Bellavance et al., 2014), in contrast to conditioning with whole-body irradiation (Priller et al., 2001; Simard and Rivest, 2004). Combining cuprizone and our chemotherapy regimen did not have a synergistic adverse effect on BBB integrity, as we could not detect any extravasation of large circulating proteins, such as albumin or IgG, into the CNS (unpublished data). Interestingly, infiltrated cells were short-lived cells as no GFP^{+} cells were observed in the CC of mice 3 wk after cuprizone removal. The transient nature of these cells suggests that they originate from monocytes rather than early myeloid progenitors introduced artificially in the bloodstream because of the BM transplantation procedure, making them actual monocyte-derived macrophages (MDMs). MDMs were shown to engraft the CNS transiently (Ajami et al., 2011), unlike uncommitted BM progenitors which are thought to engraft the brain sustainably (Davoust et al., 2008; Capotondo et al., 2012). The decline of infiltrating cells is probably caused by apoptotic processes, as is the case after experimental stroke (Li et al., 2013).

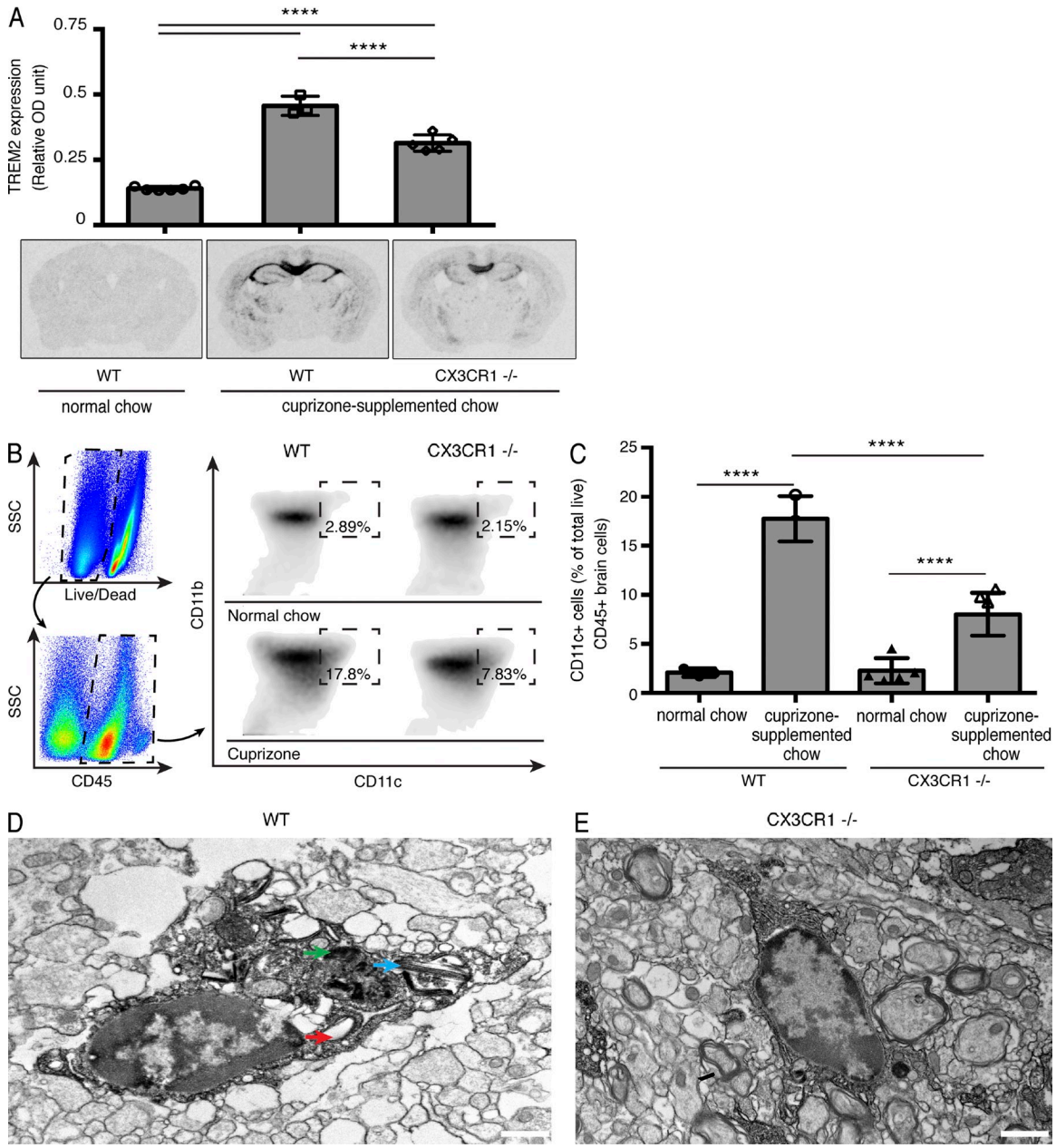

Figure 6. The phagocytic response of microglia is impaired in CX3CR1$^{-/-}$ mice after cuprizone treatment. TREM2 and CD11c expression levels were used as indicators of microglial phagocytic activity. (A) In situ hybridization signal for trem2 mRNA in the mouse brain 4 wk after the cuprizone treatment or nomal chow. (B) Flow cytometry analysis of CD11c surface protein expression in CD45$^+$ CD11b$^+$ cells in the CNS. (C) CD45$^+$ cells were selected among live cells, which were then gated against CD11b$^+$ and CD11c$^+$, cells positive for both markers are reported. (D and E) Iba1-immunoreactive signal in the brain of WT and CX3CR1$^{-/-}$ mice 5 wk after normal show or cuprizone supplemented diet. Representative electron microscopy images of microglia are shown in WT (D) and CX3CR1$^{-/-}$ (E) mice. Unstained endosomes (red arrow), partially digested myelin products localized within the endosomes (green arrow), and cholesterol crystals inside of their cytoplasm (blue arrow) were abundant in WT (D) but not in CX3CR1$^{-/-}$ microglia (E). One representative experiment out of two is shown. n = 3–6 mice/group. ****, P < 0.0001. Bars, 2 µm.

We also found that this recruitment of myeloid cells strongly depends on CCR2 signaling even though other chemokines are highly expressed during demyelination (unpublished data). Remington et al. (2007) showed that CCR2 deficiency results in lower levels of macrophages in the CC without affecting the microglial response to demyelination. Using CCR2$^{-/-}$ chimeric mice, we showed that MDMs are not actively implicated in demyelination, supporting previous observations (Mildner et al., 2007). A recent study using the lysolecithin model of demyelination suggested that monocytes are implicated in the process of remyelination as exposing old mice to a youthful hematopoietic system restored remyelination to a level similar

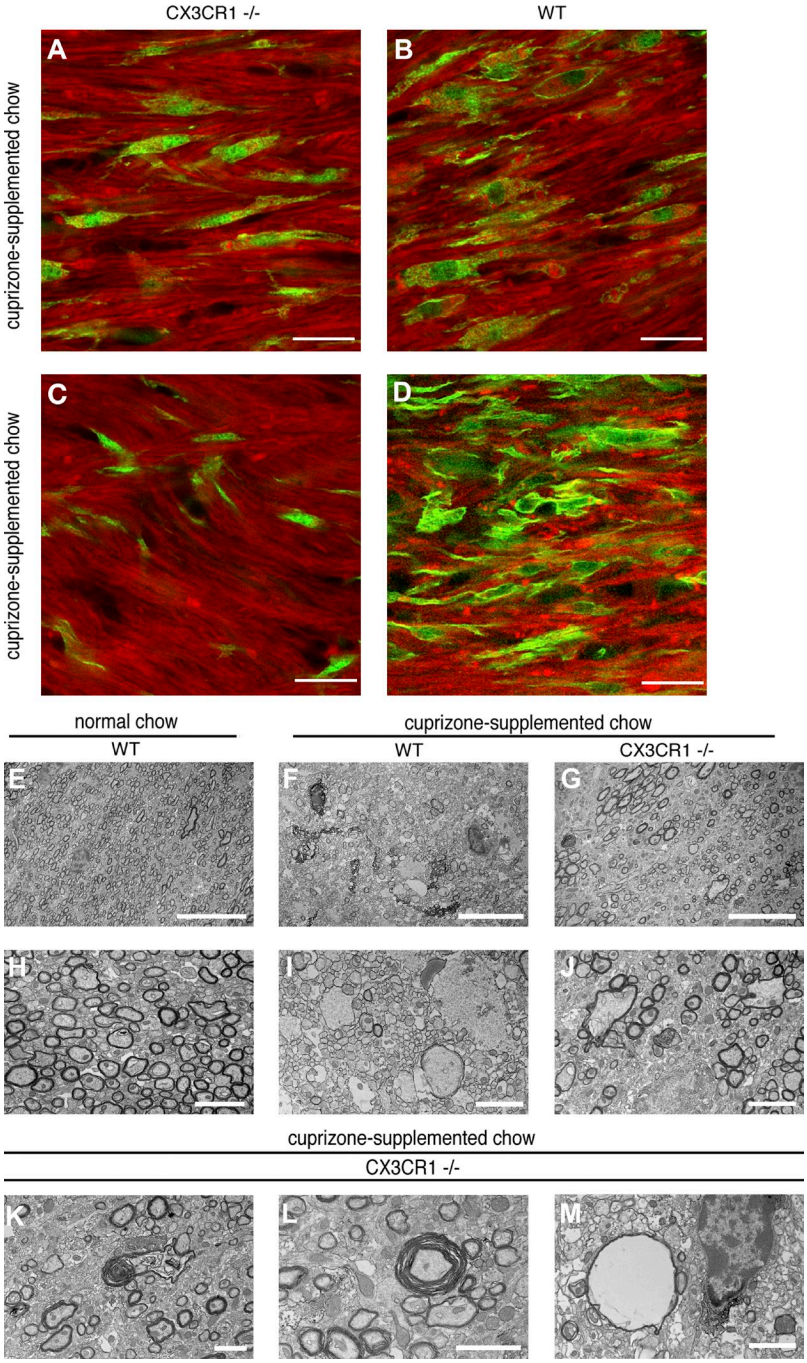

Figure 7. Myelin staining and electron microscopy reveal the presence of persistent aberrant myelin patterns in the brain of CX3CR1$^{-/-}$ mice after cuprizone feeding. (A–D) Myelin staining with 0.5 mM 1,1′-Dioctadecyl-3,3,3′,3′-tetramethylindocarbocyanine perchlorate (DiI) (red) and Iba1-immunoreactive staining (green). (E–J) Imaging at (E, F, and G) low or (H, I, and J) high magnifications of myelin state in representative sagittal microsections of the corpus callosum of either (E and H) untreated WT or (F and I) treated WT and (G and J) CX3CR1$^{-/-}$ with a cuprizone diet for 5 wk. (K–M) High powered magnification of aberrant myelin patterns frequently seen in the corpus callosum of CX3CR1$^{-/-}$ mice. Such patterns included disorganization or separation of their myelin sheath (K and L) and spheroid-like myelin-enclosed structures (M). Images were taken from mice sacrificed after 5 wk of cuprizone diet. One representative experiment out of two is shown. n = 3–6 mice/group. Bars: (A–D) 20 µm; (E–G) 5 µm; (H-M) 2 µm.

to that observed in younger animals, and the effect was dependent on CCR2 expression (Ruckh et al., 2012). Our data suggest that monocytes do not influence remyelination after cuprizone treatment as no differences were observed in mice between 1 and 2 wk after withdrawal of cuprizone from the diet. However, peripheral myeloid cells might be more involved in de- and remyelination during lysolecithin-induced demyelination compared with cuprizone because of BBB alterations resulting from the stereotactic injection of lysolecithin, permissive for the infiltration of peripheral cells in untreated controls. Whereas the role played by these cells in the cuprizone model will need to be determined, our study is, to our knowledge, the first to demonstrate controlled infiltration of MDM into the CNS in a mouse model devoid of massive neuronal death or BBB disruptions. Additional studies will be needed to firmly establish the exact role played by infiltrating macrophages in de- and remyelination processes in the brain of mice treated with cuprizone.

Microglia are actively implicated in myelin removal during demyelination (Neumann et al., 2009). The CX3CL1–CX3CR1 axis is crucial in the maintenance of microglia under a resting state because of the constant crosstalk with

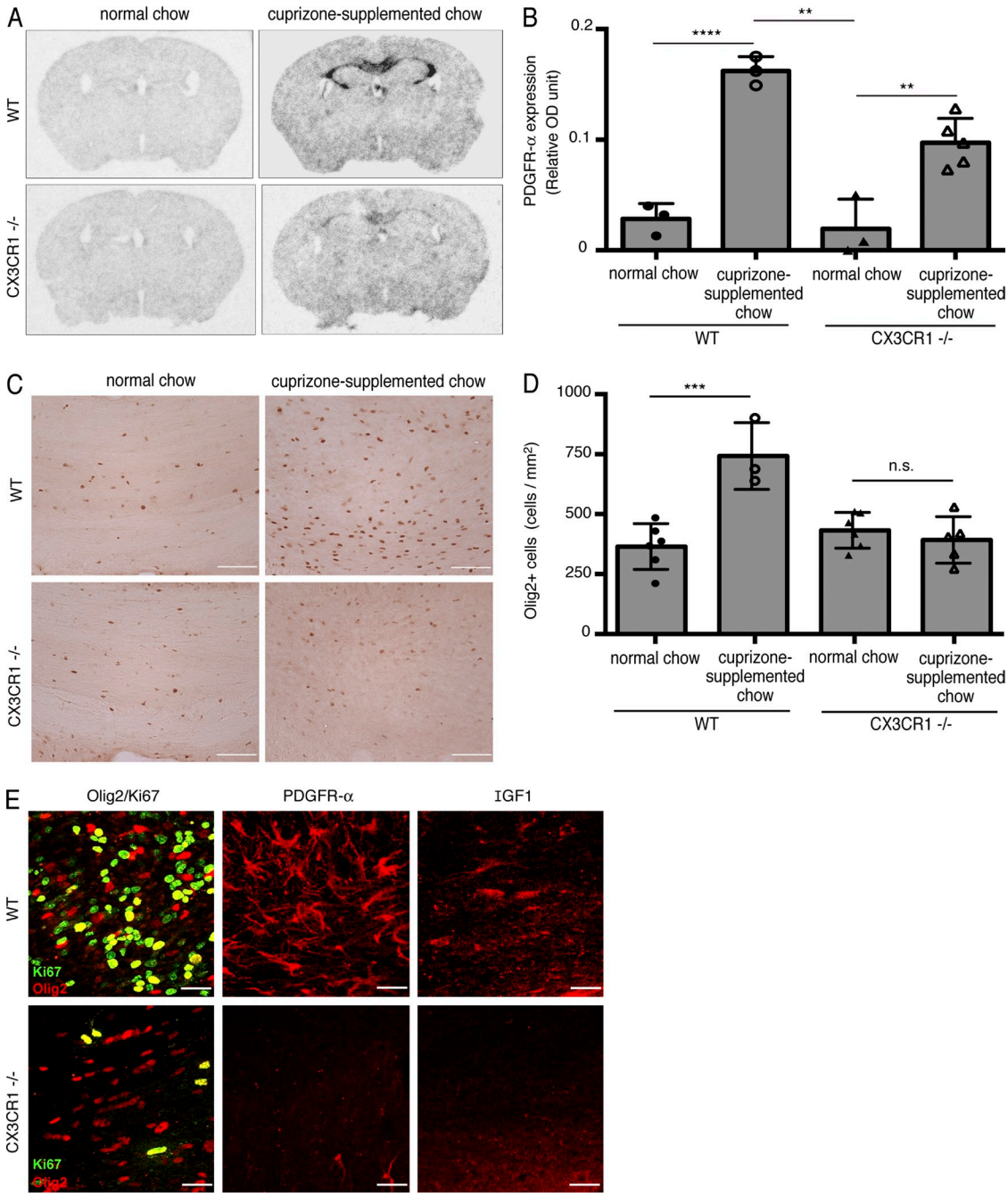

Figure 8. Demyelination-induced recruitment of oligodendrocyte precursor cells (OPCs) is impaired in CX3CR1$^{-/-}$ mice. Complementary histological markers were used to measure OPC proliferation and recruitment in the corpus callosum. (A and B) Platelet-derived growth factor receptor α (PDGFR-α) mRNA hybridization signal in the corpus callosum of mice killed 4 wk after being fed with a cuprizone-supplemented diet. (C) Representative Olig2-immunoreactive staining in the corpus callosum of WT and CX3CR1$^{-/-}$ mice 5 wk after a cuprizone treatment or normal show. (D) Stereologic quantification of Olig2-immunoreactive cells in the corpus callosum of WT and CX3CR1$^{-/-}$ after 5 wk of cuprizone or normal feeding. High expression of this protein is specific to OPCs and preoligodendrocytes (Levine et al., 2001). (E) Immunoreactive signal for Olig2 (red)/Ki67 (green), PDGFRα (red), and IGF-1 (red). One representative experiment out of two is shown. *n* = 3–6 mice/group. (B) **, P = 0.0083; ****, P < 0.0001; **, P = 0.0022; (D) ***, P = 0.0009; ***, P = 0.0003. Bars: (C) 100 µm; (E) 20 µm.

neurons (Imai et al., 1997). Its activity modulates microglial behavior both under normal and pathological conditions (Bellavance et al., 2014; Paolicelli et al., 2014). At the time points where WT mice presented severe demyelination (after 4, 5, and 6 wk of cuprizone), CX3CR1$^{-/-}$ mice showed very weak demyelination in histochemical stainings. Our data suggest that the resistance of CX3CR1$^{-/-}$ mice to demyelination does not result from a resistance to cuprizone

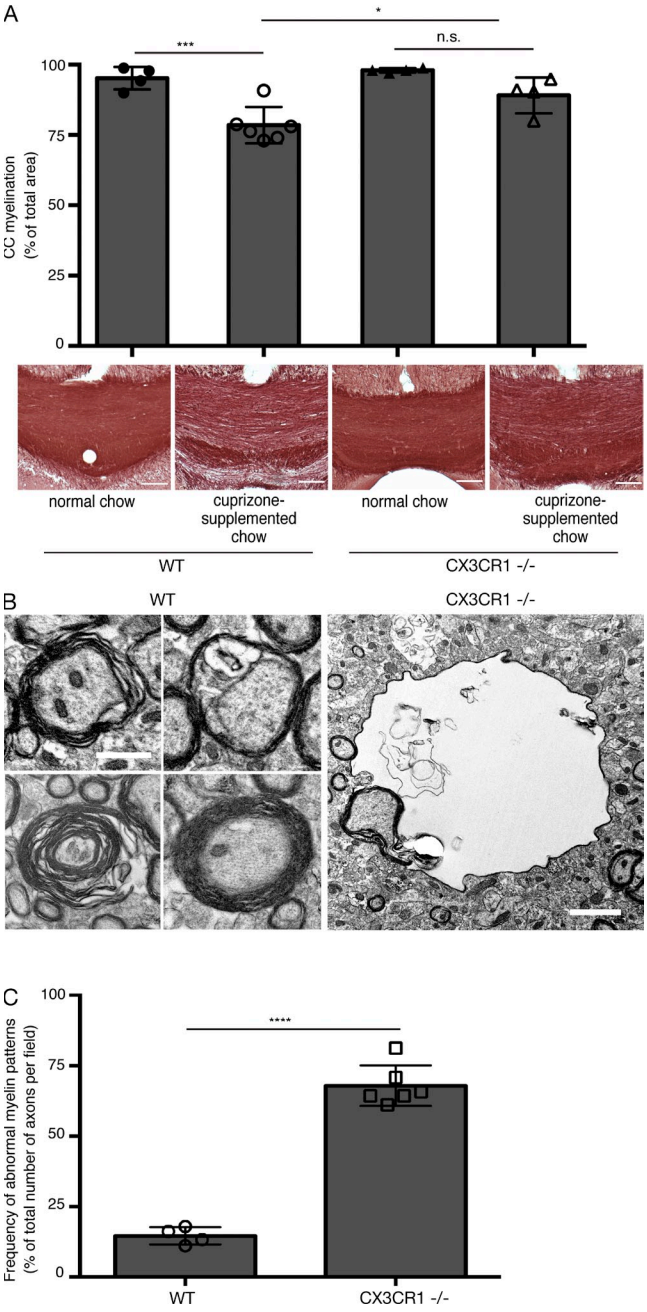

Figure 9. Persistence of myelin aberrations in CX3CR1$^{-/-}$ mice after remyelination. (A) Remyelination was assessed by the histological Black Gold staining in the corpus callosum 1 wk after cuprizone was removed from the diet. These photomicrographs are representative examples of such histological preparations for each group. Black Gold area was quantified in the corpus callosum with a stereological procedure. (B) Representative electron microscopy imaging of myelin aberrations in the corpus callosum of WT and CX3CR1$^{-/-}$ mice after remyelination. 5 wk after a cuprizone-supplemented diet, mice were killed 1 wk after normal feeding. (C) Stereologic assessment of the number of axons with aberrant myelin patterns. Presented are the means of at least three fields of view at 1900X per each animal. On average, 152 axons were counted per field of view. One representative experiment out of two is shown. *n* = 4–6 mice/group. *, P = 0.027; ***, P = 0.0010; ****, P < 0.0001. Bars: (A) 100 µm; (B) 500 nm (left); 2 µm (right).

treatment, but rather to a defect in myelin removal by CX3CR1$^{-/-}$ mice. These mice displayed both a defect in microglial migration to the CC and a defect in phagocytosis of myelin debris, whereas inflammatory responses were similar. Electron microscopy as well as myelin and Iba-1 staining revealed an almost complete absence of phagocytic inclusions in CX3CR1$^{-/-}$ microglia, unlike WT microglia that were gorged with such inclusions. This suggested that poor phagocytosis of microglial cells is the primary defect responsible for impaired clearance of myelin debris in CX3CR1$^{-/-}$ mice.

Interestingly, we observed no modulation of Cx3cl1 mRNA expression during the cuprizone treatment and no difference in its expression between WT and CX3CR1$^{-/-}$ mice (unpublished data). A link between CX3CR1 signaling and phagocytosis of debris by microglial cells has been reported in mouse models of Alzheimer's disease (AD) and excitotoxicity. In AD, it was reported that CX3CR1 deficiency enhances phagocytosis of the toxic peptide Aβ (Lee et al., 2010). As we observed during demyelination, excitotoxicity does not influence the expression of the gene encoding for CX3CL1, but promotes its cleavage from neuronal membrane (Chapman et al., 2000), resulting in a soluble isoform that promotes clearance of damaged neurons by microglia (Noda et al., 2011). The discrepancy between the effect of CX3CR1 depletion on the phagocytic capacity of microglial cells in AD and during excitotoxicity might result from the different types of phagocytosis involved (Neumann et al., 2009). Apoptotic neurons are phagocytized without inflammation via receptors like TREM-2 (Takahashi et al., 2005), which is also implicated in myelin removal during EAE (Piccio et al., 2007; Takahashi et al., 2007). Interestingly, CX3CR1$^{-/-}$ mice show a lower level of Trem2 mRNA in the CC during period of severe demyelination. However, phagocytosis of Aβ seems to depend on inflammation mediated by innate immune receptors like TLRs (Liu et al., 2005). Therefore; it is possible that CX3CR1 promotes phagocytosis of apoptotic neurons and myelin debris, but inhibits phagocytosis of Aβ. This line of thought echoes recently published results by Yamasaki et al. (Yamasaki et al., 2014) demonstrating in an EAE model that microglia actively cleared myelin debris while MDMs had other functions. However, we have shown before that MDMs were more efficient in the clearance of Aβ than resident microglia (Simard et al., 2006). It becomes tempting to suggest that microglia have evolved to become experts in dealing with products normally found in the CNS such as myelin but lack in efficiency when it comes to abnormal oligomeric aggregates like Aβ.

It will be interesting to evaluate the state of activation of CX3CR1-deficient microglial cells compared with WT as the microglial phenotype seems crucial for the promotion of OPC recruitment and tissue regeneration (Olah et al., 2012). It has been shown that microglia/macrophages exhibit a more M1-like phenotype during OPC recruitment and that there is a switch toward a M2 phenotype to allow OPC maturation (Boven et al., 2006; Miron et al., 2013). Kotter et al. showed in a series of elegant experiments that macrophages are essential

for myelin removal during demyelination (Kotter et al., 2001, 2005) and that myelin debris impair CNS remyelination by inhibiting OPC differentiation (Kotter et al., 2006). Accordingly, we expected to observe a delayed myelin clearance in CX3CR1$^{-/-}$ mice and a lower level of remyelination after removal of cuprizone from the diet when compared with WT mice, as Skripuletz et al. observed in mice devoid of astrocytes (Skripuletz et al., 2013). Surprisingly, histochemical staining revealed that, in CX3CR1$^{-/-}$ mice, remyelination occurred at a similar extent to WT mice despite lower levels of OPC in these mice after 5 wk of cuprizone. It has previously been shown that OPC density is not a rate-limiting factor for efficient remyelination (Woodruff et al., 2004). It rather seems that remyelination occurs, but in an aberrant way. Indeed, electron microscopy observations demonstrated that although CX3CR1$^{-/-}$ mice had similar numbers of myelinated axons as WT mice, a higher proportion of axons exhibited myelin abnormalities such as hypermyelination, sheath breakdown, and vacuolated formations. Studying the long-term consequences of this aberrant remyelination on axonal damages and neurological deficits may be informative.

Immunomodulators have been very efficient in the control of acute demyelinating events in relapsing–remitting courses of MS. However, these molecules have largely been ineffective in alleviating chronic demyelination in progressive forms of the disease, suggesting a primary neurodegenerative course (Stys et al., 2012). As autoimmune defects do not seem to play a significant role in progressive forms of MS, a balance between limiting demyelination and boosting remyelination of affected sites must be reached for long-term therapeutic support of these patients (Fox et al., 2012). However, the results reported in this study propose important concepts to take into consideration: there can be no efficient remyelination if microglia are unable to clear degenerate myelin from affected axons. As such, an optimal treatment strategy could consist in boosting microglial phagocytic processes whereas limiting inflammatory responses, combined with agents targeting OD physiology. Monocytes and microglia are easily targetable, even with compounds that do not cross the BBB, making them prime candidates for novel therapeutic options in progressive forms of demyelinating diseases.

MATERIALS AND METHODS

Animal care. 6–8-wk-old male C57BL/6j mice from The Jackson Laboratory were used in this study. GFP mice were crossed with CCR2$^{-/-}$ mice to generate the GFP-CCR2$^{-/-}$ mice. GFP and GFP-CCR2$^{-/-}$ mice have all C57BL/6j background and were generated from our colonies. The backcross for GFP, WT, and GFP-CCR2$^{-/-}$ were F8, F5, and F5, respectively. All animals were acclimated to standard laboratory conditions with ad libitum access to mouse chow and water. Mice were housed up to three per cage. All protocols were performed in accordance to the Canadian Council on Animal Care guidelines, as administered by the Laval University Animal Welfare Committee.

Cuprizone diet. 0.2% wt/wt cuprizone (Sigma-Aldrich) was mixed with regular ground chow and fed to experimental animals for 2, 3, 4, 5, and 6 wk. The feed was changed every 2 d and food intake was monitored throughout the protocols. Control animals were fed regular ground chow and manipulated as often as cuprizone-fed mice. For remyelination protocols, cuprizone-supplemented chow was replaced by regular chow after 6 wk and the mice were killed 1 and 2 wk later. Mice were 6–8 wk of age at the beginning of the diet. Each experiment was repeated twice.

BM transplantation. Experimental animals received a total of 80 mg/kg of Busulfan administered i.p. every 12 h for 4 d, followed by 2 d of single i.p. injections of 100 mg/kg cyclophosphamide. After a 24-h rest, 1.5–2 × 10^7 BM cells isolated from the tibia and femur of donor mice were injected into the tail vein of target animals. GFP and GFP-CCR2$^{-/-}$ mice were used as donors. For details on this procedure, please refer to previous studies (Lampron et al., 2012).

Flow cytometry. Blood samples were collected from the submandibular vein and kept from light on a rotator for <1 h. 65 µl of each blood samples was diluted with 35 µl of DPBS without Ca^{2+} or Mg^{2+} and incubated 15 min on ice with purified rat anti–mouse CD16/CD32 antibody (Mouse BD Fc Block; BD). Cells were then labeled at 4°C during 40 min with the following rat anti–mouse antibodies: V500-CD45 (clone 30-F11; BD), Alexa Fluor 700-Cd11b (clone M1/70; eBioscience), and APC-CD115 (clone AFS98; eBioscience). Next, red blood cells were lysed with BD Pharm Lyse during 20 min at room temperature, and the remaining leukocytes were washed and resuspended with DPBS w/o Ca^{2+} and Mg^{2+}. FACS and data acquisition were performed using a SORP LSR II and FACSDiva software (both from BD), respectively. Results were analyzed with the FlowJo software (Tree Star). Monocytes were identified as CD45$^+$CD11b$^+$ CD115$^+$ cells.

Brain flow cytometry. Mice were deeply anesthetized via an i.p. injection of a mixture of ketamine hydrochloride and xylazine and then perfused intracardially with ice-cold DPBS. Brains were extracted and immediately homogenized in DMEM supplemented with 10 mM Hepes and 2% FBS and filtered through a 70-µm filter. The cell suspension was then centrifugated at 300 *g* for 10 min at room temperature. After centrifugation, the supernatant was aspirated and cells were gently resuspended in 1 ml of 37% Percoll. The cell suspension was then underlaid with 70% Percoll and centrifugated at 600 *g* for 40 min with minimal acceleration and deceleration. The cell ring at the interphase was then collected and mixed thoroughly with DPBS and 2% FBS. The solution was then centrifuged at 300 *g* for 10 min and washed with DPBS + 2% FBS twice. Cells were first incubated on ice for 15 min with purified rat anti–mouse CD16/CD32 (Mouse BD Fc Block; BD). The mix was then incubated on ice with CD45-PE, CD11b-APC, and CD11c-PE (All from BD) along with the blue Live/Dead marker of cellular death (Molecular Probes) for 35 min and then washed with DPBS + 2% FBS. The cells were analyzed using a two-laser, six-color FACS Canto II flow cytometer and data acquisition was done with BD FACSDiva software (Version 6.1.2; BD). Cells were then acquired according to the different fluorescent antibodies. Results were analyzed using FlowJo software (Tree Star).

Immunohistochemistry. To collect the brain tissues, mice were deeply anesthetized via an i.p. injection of a mixture of ketamine hydrochloride and xylazine, and then rapidly perfused transcardially with 0.9% saline, followed by 4% paraformaldehyde in sodium phosphate buffer (pH 7.4 at 4°C). Brains were rapidly removed from the skulls, postfixed overnight, and then placed in a solution containing 10% sucrose diluted in 4% paraformaldehyde (pH 7.4) for at least 48 h at 4°C. The frozen brains were mounted on a microtome (Reichert-Jung; Cambridge Instruments Company), frozen with dry ice, and cut into 25-µm coronal sections from the olfactory bulb to the end of the medulla. The slices were collected in a cold cryoprotectant solution (0.05 M sodium phosphate buffer, pH 7.3, 30% ethylene glycol, 20% glycerol) and stored at −20°C. Free-floating sections were incubated for 30 min in KPBS containing 4% goat serum, 1% BSA, and 0.4% Triton X-100. Using the same blocking solution, the sections were then incubated overnight in primary Ab at 4°C. The sections were then rinsed four times for 5 min in KPBS, followed by a 90 min incubation in fluorochrome- or biotin-conjugated goat secondary anitbody at room temperature. For multiple stainings, the previous wash and incubation steps were repeated with the other antibodies.

For nonfluorescent staining, biotin-conjugated secondary Ab were detected using the peroxidase-based Vectastain ABC kit (Vector Labs) following the manufacturer's instructions. Sections were then rinsed four times for 5 min in KPBS, revealed with 3,3′-Diaminobenzidine tetrahydrochloride (Sigma-Aldrich) and mounted onto SuperFrost slides (Thermo Fisher Scientific), stained with DAPI if needed (0.0002% dilution for 10 min; Molecular Probes), and coverslipped with antifade medium composed of 96 mM Tris-Hcl, pH 8.0, 24% glycerol, 9.6% polyvinylalcohol, and 2.5% diazabicyclooctane (Sigma-Aldrich) or DPX mountant (Electron Microscopy Science). Confocal laser scanning microscopy was performed with a BX-61 microscope equipped with the Fluoview SV500 imaging software 4.3 (Olympus America Inc.). Confocal images were acquired by sequential scanning using a two-frame Kalman filter and a z-separation of 1 µm. Image mosaics were acquired using Micro-Manager software (version 1.3.36 β) with an Olympus IX81 microscope, equipped with a 4X lens, a GFP filter, a Prior ProScan motorized stage and a Qimaging Retiga EXi digital camera. Acquired images were thereafter stitched together using XuvStitch x64 software (version 1.8.0; Emmenlauer et al., 2009) and exported as hdf5 files, then converted to tiff with ImageJ x64 software (version 1.46m; Schneider et al., 2012). Stereological analysis was performed as previously described (Simard et al., 2006). Contours of regions of interest were traced as virtual overlay on the streamed images. Individual cells were counted and reported as a density of events in relation to the surface of the area containing them.

Myelin staining. Free floating tissue sections were incubated 30 min in 0.5 mM 1,1′-Dioctadecyl-3,3,3′,3′-tetramethylindocarbocyanine perchlorate or DiI (Sigma-Aldrich) in the blocking solution, which was followed by 3 washing steps in KPBS (see previous section).

Black Gold staining and quantification of myelination. Brain sections collected as described above were washed three times for 10 min in cold KPBS. 3–4 slices of interest were then put into a 1.5 mL sample tube (Eppendorf) containing 200 µL of Black Gold (EMD Millipore) diluted 0.3% into 0.9% NaCl. These were incubated exactly 10 min at 62°C, transferred to KPBS, mounted onto Superfrost slides, and coverslipped, as described above. 8-bit grayscale TIFF images of the regions of interest were taken in a single sitting for whole protocols with a Qimaging camera, with the same gain/exposure settings for every image. To quantify myelination, these images were imported into ImageJ and myelination of a given area was measured as the surface proportion of staining intensity above a determined threshold. This threshold was set to detect at least 95% of myelination in untreated WT controls and average 30% in WT mice treated for 3, 5, 6, and 7 wk.

Behavior analysis. Elevated plus maze was used to quantify behavioral deficits in cuprizone-treated mice as previously described (Walf and Frye, 2007). The elevated plus-maze was made of beige Plexiglas illuminated under constant, homogenous lighting (350 lux). The apparatus consisted of four arms (30 × 5 cm) elevated 40 cm above floor level. Two of the arms contained 15-cm-high walls (enclosed arms) and the other two contained none (open arms). Each mouse was placed in the middle section facing an open arm and left to explore the maze for a single 5-min session with the experimenter out of view. After each trial, the floor was wiped clean with a damp cloth and dried. The following scores were taken: open arm entries and duration (inversely related to anxiety) and distance traveled (reflecting general ambulation), measured by a video camera and analyzed with a video tracking system (ANY-maze; Stoelting Co.), which considers an animal inside a zone whenever its center point is within it.

In situ hybridization. In situ hybridization was performed on every twelfth section of the brain, starting from the end of the olfactory bulb to the end of the cortex, using 35S-labeled cRNA probes as described previously (Laflamme and Rivest, 2001).

Fluoro-Jade B staining. Neuronal death was labeled with the Fluoro-Jade B (FJB) method. In brief, every sixth section of the whole rostrocaudal extent of each brain was mounted onto Superfrost slides (Thermo Fisher Scientific), dried under vacuum for 2 h, dehydrated through graded concentrations of alcohol (50, 70, and 100% for 1 min each), and rehydrated through graded concentrations of alcohol (100, 70, and 50% for 1 min each) and 1 min in distillated water. They were then dipped into and shaken in potassium permanganate (0.06%) for 10 min, rinsed for 1 min in distillated water, and dipped into and shaken in a solution containing Fluoro–Jade B (Fluoro–Jade B 0.0004% [Histochem] + acetic acid 0.1% [Sigma-Aldrich] + DAPI 0.0002% [Molecular Probes]) for 20 min. The slides were thereafter rinsed three times in distillated water (1 min each), dried, dipped in xylene three times (2 min each), and coverslipped with DPX.

Immunoelectron microscopy. Mice were deeply anesthetized with sodium pentobarbital (80 mg/kg, i.p.) and perfused through the aortic arch with 3.5% acrolein (in 100 mM phosphate buffer [PB], pH 7.4) followed by 4% paraformaldehyde (PFA; in 100 mM PB, pH 7.4). Longitudinal sections of the brain (50 µm thick) were cut with a vibratome in ice-cooled PBS (0.9% NaCl in 50 mM phosphate buffer, pH 7.4) and immunostained with a rabbit anti-ionized calcium binding adaptor molecule 1 (IBA1) antibody (1:1,000 in blocking solution; Wako Pure Chemical Industries) as previously described (Tremblay et al., 2010). In brief, labeling was revealed with 3,3′-Diaminobenzidine tetrahydrochloride (DAB; 0.05 mg/ml) and hydrogen peroxide (0.03% in buffer solution; DAB Peroxidase Substrate kit; Vector Laboratories). Immunostained sections were postfixed flat in 1% osmium tetroxide, dehydrated in ascending concentrations of ethanol, impregnated in Durcupan (Electron Microscopy Sciences) overnight at room temperature, mounted between ACLAR-embedding films (Electron Microscopy Sciences), and cured at 55°C for 48 h. Areas of the corpus callosum were excised from the embedded sections, reembedded at the tip of resin blocks, cut with an ultra-microtome (Leica Ultracut S) at 65–80 nm thickness, collected on bare square-mesh grids, and examined with an FEI Tecnai G2 Spirit BioTwin electron microscope.

Statistical analysis. Data are presented as mean ± SEM. Statistical tests performed include two-tailed unpaired Student's *t* test using Welch's correction of unequal variances and 1-way ANOVA followed by Tukey or Bonferroni post-hoc test for multiple comparisons. All analyses were carried with the Prism software (version 6; GraphPad) and the α level was set at 0.05.

Online supplemental material. Fig. S1 shows food intake and body weight throughout a cuprizone protocol and Video 1 shows sequential images from deep corpus callosum by confocal microscopy. Online supplemental material is available at http://www.jem.org/cgi/content/full/jem.20141656/DC1.

The authors would like to thank Dr. Denis Soulet for his technical help in preparing the stitched image mosaic.

This work was supported by grants from the Canadian Institutes for Health Research and the Multiple Sclerosis Scientific Research Foundation of Canada.

The authors have no conflicting financial interests.

Submitted: 26 August 2014
Accepted: 9 February 2015

REFERENCES

Ajami, B., J.L. Bennett, C. Krieger, W. Tetzlaff, and F.M.V. Rossi. 2007. Local self-renewal can sustain CNS microglia maintenance and function throughout adult life. *Nat. Neurosci.* 10:1538–1543. http://dx.doi.org/10.1038/nn2014

Ajami, B., J.L. Bennett, C. Krieger, K.M. McNagny, and F.M.V. Rossi. 2011. Infiltrating monocytes trigger EAE progression, but do not contribute to the resident microglia pool. *Nat. Neurosci.* 14:1142–1149. http://dx.doi.org/10.1038/nn.2887

Arnett, H.A., J. Mason, M. Marino, K. Suzuki, G.K. Matsushima, and J.P. Ting. 2001. TNF alpha promotes proliferation of oligodendrocyte progenitors and remyelination. *Nat. Neurosci.* 4:1116–1122. http://dx.doi.org/10.1038/nn738

Bakker, D.A., and S.K. Ludwin. 1987. Blood-brain barrier permeability during Cuprizone-induced demyelination. Implications for the pathogenesis of immune-mediated demyelinating diseases. *J. Neurol. Sci.* 78:125–137. http://dx.doi.org/10.1016/0022-510X(87)90055-4

Bellavance, M.-A., D. Gosselin, V.W. Yong, P.K. Stys, and S. Rivest. 2014. Patrolling monocytes play a critical role in CX3CR1-mediated neuroprotection during excitotoxicity. *Brain Struct. Funct.* http://dx.doi.org/10.1007/s00429-014-0759-z

Bénardais, K., A. Kotsiari, J. Skuljec, P.N. Koutsoudaki, V. Gudi, V. Singh, F. Vulinović, T. Skripuletz, and M. Stangel. 2013. Cuprizone [bis(cyclohexylidenehydrazide)] is selectively toxic for mature oligodendrocytes. *Neurotox. Res.* 24:244–250. http://dx.doi.org/10.1007/s12640-013-9380-9

Blakemore, W.F., and K.A. Irvine. 2008. Endogenous or exogenous oligodendrocytes for remyelination. *J. Neurol. Sci.* 265:43–46. http://dx.doi.org/10.1016/j.jns.2007.08.004

Boven, L.A., M. Van Meurs, M. Van Zwam, A. Wierenga-Wolf, R.Q. Hintzen, R.G. Boot, J.M. Aerts, S. Amor, E.E. Nieuwenhuis, and J.D. Laman. 2006. Myelin-laden macrophages are anti-inflammatory, consistent with foam cells in multiple sclerosis. *Brain.* 129:517–526. http://dx.doi.org/10.1093/brain/awh707

Capotondo, A., R. Milazzo, L.S. Politi, A. Quattrini, A. Palini, T. Plati, S. Merella, A. Nonis, C. di Serio, E. Montini, et al. 2012. Brain conditioning is instrumental for successful microglia reconstitution following hematopoietic stem cell transplantation. *Proc. Natl. Acad. Sci. USA.* 109:15018–15023. http://dx.doi.org/10.1073/pnas.1205858109

Cardona, A.E., E.P. Pioro, M.E. Sasse, V. Kostenko, S.M. Cardona, I.M. Dijkstra, D. Huang, G. Kidd, S. Dombrowski, R. Dutta, et al. 2006. Control of microglial neurotoxicity by the fractalkine receptor. *Nat. Neurosci.* 9:917–924. http://dx.doi.org/10.1038/nn1715

Chapman, G.A., K. Moores, D. Harrison, C.A. Campbell, B.R. Stewart, and P.J. Strijbos. 2000. Fractalkine cleavage from neuronal membranes represents an acute event in the inflammatory response to excitotoxic brain damage. *J. Neurosci.* 20:RC87.

Davoust, N., C. Vuaillat, G. Androdias, and S. Nataf. 2008. From bone marrow to microglia: barriers and avenues. *Trends Immunol.* 29:227–234. http://dx.doi.org/10.1016/j.it.2008.01.010

Deshmukh, V.A., V. Tardif, C.A. Lyssiotis, C.C. Green, B. Kerman, H.J. Kim, K. Padmanabhan, J.G. Swoboda, I. Ahmad, T. Kondo, et al. 2013. A regenerative approach to the treatment of multiple sclerosis. *Nature.* 502:327–332. http://dx.doi.org/10.1038/nature12647

Emmenlauer, M., O. Ronneberger, A. Ponti, P. Schwarb, A. Griffa, A. Filippi, R. Nitschke, W. Driever, and H. Burkhardt. 2009. XuvTools: free, fast and reliable stitching of large 3D datasets. *J. Microsc.* 233:42–60. http://dx.doi.org/10.1111/j.1365-2818.2008.03094.x

Ferguson, B., M.K. Matyszak, M.M. Esiri, and V.H. Perry. 1997. Axonal damage in acute multiple sclerosis lesions. *Brain.* 120:393–399. http://dx.doi.org/10.1093/brain/120.3.393

Fife, B.T., G.B. Huffnagle, W.A. Kuziel, and W.J. Karpus. 2000. CC chemokine receptor 2 is critical for induction of experimental autoimmune encephalomyelitis. *J. Exp. Med.* 192:899–905. http://dx.doi.org/10.1084/jem.192.6.899

Fox, R.J., A. Thompson, D. Baker, P. Baneke, D. Brown, P. Browne, D. Chandraratna, O. Ciccarelli, T. Coetzee, G. Comi, et al. 2012. Setting a research agenda for progressive multiple sclerosis: the International Collaborative on Progressive MS. *Mult. Scler.* 18:1534–1540. http://dx.doi.org/10.1177/1352458512458169

Franklin, R.J.M., and C. Ffrench-Constant. 2008. Remyelination in the CNS: from biology to therapy. *Nat. Rev. Neurosci.* 9:839–855. http://dx.doi.org/10.1038/nrn2480

Geissmann, F., M.G. Manz, S. Jung, M.H. Sieweke, M. Merad, and K. Ley. 2010. Development of monocytes, macrophages, and dendritic cells. *Science.* 327:656–661. http://dx.doi.org/10.1126/science.1178331

Ginhoux, F., M. Greter, M. Leboeuf, S. Nandi, P. See, S. Gokhan, M.F. Mehler, S.J. Conway, L.G. Ng, E.R. Stanley, et al. 2010. Fate mapping analysis reveals that adult microglia derive from primitive macrophages. *Science.* 330:841–845. http://dx.doi.org/10.1126/science.1194637

Goldschmidt, T., J. Antel, F.B. König, W. Brück, and T. Kuhlmann. 2009. Remyelination capacity of the MS brain decreases with disease chronicity. *Neurology.* 72:1914–1921. http://dx.doi.org/10.1212/WNL.0b013e3181a8260a

Gudi, V., S. Gingele, T. Skripuletz, and M. Stangel. 2014. Glial response during cuprizone-induced de- and remyelination in the CNS: lessons learned. *Front. Cell. Neurosci.* 8:73. http://dx.doi.org/10.3389/fncel.2014.00073

Heppner, F.L., M. Greter, D. Marino, J. Falsig, G. Raivich, N. Hövelmeyer, A. Waisman, T. Rülicke, M. Prinz, J. Priller, et al. 2005. Experimental autoimmune encephalomyelitis repressed by microglial paralysis. *Nat. Med.* 11:146–152. http://dx.doi.org/10.1038/nm1177

Hiremath, M.M., Y. Saito, G.W. Knapp, J.P. Ting, K. Suzuki, and G.K. Matsushima. 1998. Microglial/macrophage accumulation during cuprizone-induced demyelination in C57BL/6 mice. *J. Neuroimmunol.* 92:38–49. http://dx.doi.org/10.1016/S0165-5728(98)00168-4

Imai, T., K. Hieshima, C. Haskell, M. Baba, M. Nagira, M. Nishimura, M. Kakizaki, S. Takagi, H. Nomiyama, T.J. Schall, and O. Yoshie. 1997. Identification and molecular characterization of fractalkine receptor CX3CR1, which mediates both leukocyte migration and adhesion. *Cell.* 91:521–530. http://dx.doi.org/10.1016/S0092-8674(00)80438-9

Jurevics, H., C. Largent, J. Hostettler, D.W. Sammond, G.K. Matsushima, A. Kleindienst, A.D. Toews, and P. Morell. 2002. Alterations in metabolism and gene expression in brain regions during cuprizone-induced demyelination and remyelination. *J. Neurochem.* 82:126–136. http://dx.doi.org/10.1046/j.1471-4159.2002.00954.x

Klinkner, A.M., C.R. Waites, W.D. Kerns, and P.J. Bugelski. 1995. Evidence of foam cell and cholesterol crystal formation in macrophages incubated with oxidized LDL by fluorescence and electron microscopy. *J. Histochem. Cytochem.* 43:1071–1078. http://dx.doi.org/10.1177/43.10.7560885

Kondo, A., T. Nakano, and K. Suzuki. 1987. Blood-brain barrier permeability to horseradish peroxidase in twitcher and cuprizone-intoxicated mice. *Brain Res.* 425:186–190. http://dx.doi.org/10.1016/0006-8993(87)90499-9

Kotter, M.R., A. Setzu, F.J. Sim, N. Van Rooijen, and R.J. Franklin. 2001. Macrophage depletion impairs oligodendrocyte remyelination following lysolecithin-induced demyelination. *Glia.* 35:204–212. http://dx.doi.org/10.1002/glia.1085

Kotter, M.R., C. Zhao, N. van Rooijen, and R.J.M. Franklin. 2005. Macrophage-depletion induced impairment of experimental CNS remyelination is associated with a reduced oligodendrocyte progenitor cell response and altered growth factor expression. *Neurobiol. Dis.* 18:166–175. http://dx.doi.org/10.1016/j.nbd.2004.09.019

Kotter, M.R., W.-W. Li, C. Zhao, and R.J.M. Franklin. 2006. Myelin impairs CNS remyelination by inhibiting oligodendrocyte precursor cell differentiation. *J. Neurosci.* 26:328–332. http://dx.doi.org/10.1523/JNEUROSCI.2615-05.2006

Laflamme, N., and S. Rivest. 2001. Toll-like receptor 4: the missing link of the cerebral innate immune response triggered by circulating gram-negative bacterial cell wall components. *FASEB J.* 15:155–163. http://dx.doi.org/10.1096/fj.00-0339com

Lampron, A., M. Lessard, and S. Rivest. 2012. Effects of myeloablation, peripheral chimerism, and whole-body irradiation on the entry of bone marrow-derived cells into the brain. *Cell Transplant.* 21:1149–1159. http://dx.doi.org/10.3727/096368911X593154

Lampron, A., P.M. Pimentel-Coelho, and S. Rivest. 2013. Migration of bone marrow-derived cells into the central nervous system in models of neurodegeneration. *J. Comp. Neurol.* 521:3863–3876.

Lassmann, H., J. van Horssen, and D. Mahad. 2012. Progressive multiple sclerosis: pathology and pathogenesis. *Nat. Rev. Neurol.* 8:647–656. http://dx.doi.org/10.1038/nrneurol.2012.168

Lee, S., N.H. Varvel, M.E. Konerth, G. Xu, A.E. Cardona, R.M. Ransohoff, and B.T. Lamb. 2010. CX3CR1 deficiency alters microglial activation and reduces beta-amyloid deposition in two Alzheimer's disease mouse models. *Am. J. Pathol.* 177:2549–2562. http://dx.doi.org/10.2353/ajpath.2010.100265

Levine, J.M., R. Reynolds, and J.W. Fawcett. 2001. The oligodendrocyte precursor cell in health and disease. *Trends Neurosci.* 24:39–47. http://www.sciencedirect.com/science/article/pii/S016622360001691X?

Li, T., S. Pang, Y. Yu, X. Wu, J. Guo, and S. Zhang. 2013. Proliferation of parenchymal microglia is the main source of microgliosis after ischaemic stroke. *Brain.* 136:3578–3588. http://dx.doi.org/10.1093/brain/awt287

Lindberg, O.R., A. Brederlau, and H.G. Kuhn. 2014. Epidermal growth factor treatment of the adult brain subventricular zone leads to focal

microglia/macrophage accumulation and angiogenesis. *Stem Cell Rev.* 2:440–448. http://dx.doi.org/10.1016/j.stemcr.2014.02.003

Lister, R.G. 1987. The use of a plus-maze to measure anxiety in the mouse. *Psychopharmacology (Berl.).* 92:180–185. http://dx.doi.org/10.1007/BF00177912

Liu, Y., S. Walter, M. Stagi, D. Cherny, M. Letiembre, W. Schulz-Schaeffer, H. Heine, B. Penke, H. Neumann, and K. Fassbender. 2005. LPS receptor (CD14): a receptor for phagocytosis of Alzheimer's amyloid peptide. *Brain.* 128:1778–1789. http://dx.doi.org/10.1093/brain/awh531

Lublin, F.D., and S.C. Reingold. National Multiple Sclerosis Society (USA) Advisory Committee on Clinical Trials of New Agents in Multiple Sclerosis. 1996. Defining the clinical course of multiple sclerosis: results of an international survey. *Neurology.* 46:907–911. http://dx.doi.org/10.1212/WNL.46.4.907

Lublin, F.D., S.C. Reingold, J.A. Cohen, G.R. Cutter, P.S. Sørensen, A.J. Thompson, J.S. Wolinsky, L.J. Balcer, B. Banwell, F. Barkhof, et al. 2014. Defining the clinical course of multiple sclerosis: the 2013 revisions. *Neurology.* 83:278–286. http://dx.doi.org/10.1212/WNL.0000000000000560

Matsushima, G.K., and P. Morell. 2001. The neurotoxicant, cuprizone, as a model to study demyelination and remyelination in the central nervous system. *Brain Pathol.* 11:107–116. http://dx.doi.org/10.1111/j.1750-3639.2001.tb00385.x

McMahon, E.J., K. Suzuki, and G.K. Matsushima. 2002. Peripheral macrophage recruitment in cuprizone-induced CNS demyelination despite an intact blood-brain barrier. *J. Neuroimmunol.* 130:32–45. http://dx.doi.org/10.1016/S0165-5728(02)00205-9

Michaud, J.-P., M.-A. Bellavance, P. Préfontaine, and S. Rivest. 2013. Real-time in vivo imaging reveals the ability of monocytes to clear vascular amyloid beta. *Cell Reports.* 5:646–653. http://dx.doi.org/10.1016/j.celrep.2013.10.010

Mildner, A., H. Schmidt, M. Nitsche, D. Merkler, U.-K. Hanisch, M. Mack, M. Heikenwalder, W. Brück, J. Priller, and M. Prinz. 2007. Microglia in the adult brain arise from Ly-6ChiCCR2+ monocytes only under defined host conditions. *Nat. Neurosci.* 10:1544–1553. http://dx.doi.org/10.1038/nn2015

Miron, V.E., A. Boyd, J.-W. Zhao, T.J. Yuen, J.M. Ruckh, J.L. Shadrach, P. van Wijngaarden, A.J. Wagers, A. Williams, R.J.M. Franklin, and C. ffrench-Constant. 2013. M2 microglia and macrophages drive oligodendrocyte differentiation during CNS remyelination. *Nat. Neurosci.* 16:1211–1218. http://dx.doi.org/10.1038/nn.3469

Napoli, I., and H. Neumann. 2010. Protective effects of microglia in multiple sclerosis. *Exp. Neurol.* 225:24–28. http://dx.doi.org/10.1016/j.expneurol.2009.04.024

Neumann, H., M.R. Kotter, and R.J.M. Franklin. 2009. Debris clearance by microglia: an essential link between degeneration and regeneration. *Brain.* 132:288–295. http://dx.doi.org/10.1093/brain/awn109

Noda, M., Y. Doi, J. Liang, J. Kawanokuchi, Y. Sonobe, H. Takeuchi, T. Mizuno, and A. Suzumura. 2011. Fractalkine attenuates excito-neurotoxicity via microglial clearance of damaged neurons and antioxidant enzyme heme oxygenase-1 expression. *J. Biol. Chem.* 286:2308–2319. http://dx.doi.org/10.1074/jbc.M110.169839

Olah, M., S. Amor, N. Brouwer, J. Vinet, B. Eggen, K. Biber, and H.W.G.M. Boddeke. 2012. Identification of a microglia phenotype supportive of remyelination. *Glia.* 60:306–321. http://dx.doi.org/10.1002/glia.21266

Paolicelli, R.C., K. Bisht, and M.-È. Tremblay. 2014. Fractalkine regulation of microglial physiology and consequences on the brain and behavior. *Front. Cell. Neurosci.* 8:129. http://dx.doi.org/10.3389/fncel.2014.00129

Piccio, L., C. Buonsanti, M. Mariani, M. Cella, S. Gilfillan, A.H. Cross, M. Colonna, and P. Panina-Bordignon. 2007. Blockade of TREM-2 exacerbates experimental autoimmune encephalomyelitis. *Eur. J. Immunol.* 37:1290–1301. http://dx.doi.org/10.1002/eji.200636837

Priller, J., D.A. Persons, F.F. Klett, G. Kempermann, G.W. Kreutzberg, and U. Dirnagl. 2001. Neogenesis of cerebellar Purkinje neurons from gene-marked bone marrow cells in vivo. *J. Cell Biol.* 155:733–738. http://dx.doi.org/10.1083/jcb.200105103

Pulford, K.A., A. Sipos, J.L. Cordell, W.P. Stross, and D.Y. Mason. 1990. Distribution of the CD68 macrophage/myeloid associated antigen. *Int. Immunol.* 2:973–980. http://dx.doi.org/10.1093/intimm/2.10.973

Remington, L.T., A.A. Babcock, S.P. Zehntner, and T. Owens. 2007. Microglial recruitment, activation, and proliferation in response to primary demyelination. *Am. J. Pathol.* 170:1713–1724. http://dx.doi.org/10.2353/ajpath.2007.060783

Ruckh, J.M., J.-W. Zhao, J.L. Shadrach, P. van Wijngaarden, T.N. Rao, A.J. Wagers, and R.J.M. Franklin. 2012. Rejuvenation of regeneration in the aging central nervous system. *Cell Stem Cell.* 10:96–103. http://dx.doi.org/10.1016/j.stem.2011.11.019

Schneider, C.A., W.S. Rasband, and K.W. Eliceiri. 2012. NIH Image to ImageJ: 25 years of image analysis. *Nat. Methods.* 9:671–675. http://dx.doi.org/10.1038/nmeth.2089

Schulz, C., E. Gomez Perdiguero, L. Chorro, H. Szabo-Rogers, N. Cagnard, K. Kierdorf, M. Prinz, B. Wu, S.E.W. Jacobsen, J.W. Pollard, et al. 2012. A lineage of myeloid cells independent of Myb and hematopoietic stem cells. *Science.* 336:86–90. http://dx.doi.org/10.1126/science.1219179

Shechter, R., A. London, C. Varol, C. Raposo, M. Cusimano, G. Yovel, A. Rolls, M. Mack, S. Pluchino, G. Martino, et al. 2009. Infiltrating blood-derived macrophages are vital cells playing an anti-inflammatory role in recovery from spinal cord injury in mice. *PLoS Med.* 6:e1000113. http://dx.doi.org/10.1371/journal.pmed.1000113

Simard, A.R., and S. Rivest. 2004. Bone marrow stem cells have the ability to populate the entire central nervous system into fully differentiated parenchymal microglia. *FASEB J.* 18:998–1000.

Simard, A.R., D. Soulet, G. Gowing, J.-P. Julien, and S. Rivest. 2006. Bone marrow-derived microglia play a critical role in restricting senile plaque formation in Alzheimer's disease. *Neuron.* 49:489–502. http://dx.doi.org/10.1016/j.neuron.2006.01.022

Skripuletz, T., D. Hackstette, K. Bauer, V. Gudi, R. Pul, E. Voss, K. Berger, M. Kipp, W. Baumgärtner, and M. Stangel. 2013. Astrocytes regulate myelin clearance through recruitment of microglia during cuprizone-induced demyelination. *Brain.* 136:147–167. http://dx.doi.org/10.1093/brain/aws262

Stirling, D.P., K. Cummins, M. Mishra, W. Teo, V.W. Yong, and P. Stys. 2013. Toll-like receptor 2-mediated alternative activation of microglia is protective after spinal cord injury. *Brain.* 137:707–723. http://dx.doi.org/10.1093/brain/awt341

Stys, P.K., G.W. Zamponi, J. van Minnen, and J.J.G. Geurts. 2012. Will the real multiple sclerosis please stand up? *Nat. Rev. Neurosci.* 13:507–514. http://dx.doi.org/10.1038/nrn3275

Takahashi, K., C.D.P. Rochford, and H. Neumann. 2005. Clearance of apoptotic neurons without inflammation by microglial triggering receptor expressed on myeloid cells-2. *J. Exp. Med.* 201:647–657. http://dx.doi.org/10.1084/jem.20041611

Takahashi, K., M. Prinz, M. Stagi, O. Chechneva, and H. Neumann. 2007. TREM2-transduced myeloid precursors mediate nervous tissue debris clearance and facilitate recovery in an animal model of multiple sclerosis. *PLoS Med.* 4:e124. http://dx.doi.org/10.1371/journal.pmed.0040124

Tangirala, R.K., W.G. Jerome, N.L. Jones, D.M. Small, W.J. Johnson, J.M. Glick, F.H. Mahlberg, and G.H. Rothblat. 1994. Formation of cholesterol monohydrate crystals in macrophage-derived foam cells. *J. Lipid Res.* 35:93–104.

Trapp, B.D., J. Peterson, R.M. Ransohoff, R. Rudick, S. Mörk, and L. Bö. 1998. Axonal transection in the lesions of multiple sclerosis. *N. Engl. J. Med.* 338:278–285. http://dx.doi.org/10.1056/NEJM199801293380502

Tremblay, M.-È., M. Riad, and A. Majewska. 2010. Preparation of mouse brain tissue for immunoelectron microscopy. *J. Vis. Exp.* (41). http://dx.doi.org/10.3791/2021

Walf, A.A., and C.A. Frye. 2007. The use of the elevated plus maze as an assay of anxiety-related behavior in rodents. *Nat. Protoc.* 2:322–328. http://dx.doi.org/10.1038/nprot.2007.44

Woodruff, R.H., M. Fruttiger, W.D. Richardson, and R.J.M. Franklin. 2004. Platelet-derived growth factor regulates oligodendrocyte progenitor numbers in adult CNS and their response following CNS demyelination. *Mol. Cell. Neurosci.* 25:252–262. http://dx.doi.org/10.1016/j.mcn.2003.10.014

Yamasaki, R., H. Lu, O. Butovsky, N. Ohno, A.M. Rietsch, R. Cialic, P.M. Wu, C.E. Doykan, J. Lin, A.C. Cotleur, et al. 2014. Differential roles of microglia and monocytes in the inflamed central nervous system. *J. Exp. Med.* 211:1533–1549. http://dx.doi.org/10.1084/jem.20132477